An Intelligent Overcurrent Protection Algorithm of Distribution Systems with Inverter based Distributed Energy Resources

Lina He
Department of Electrical and Computer Engineering
University of Illinois at Chicago
Chicago, USA
lhe@uic.edu

Shuaiang Rong
Department of Electrical and Computer Engineering
University of Illinois at Chicago
Chicago, USA
srong4@uic.edu

Chengwei Liu
Department of School of Electrical and Electronic Engineering
Huazhong University of Science & Technology
Wuhan, China
u201611938@hust.edu.cn

Abstract—**To facilitate renewable energy, distributed energy resources (DERs) have been significantly integrated into distribution systems through power electronics-based inverters. The control of these inverters can limit the fault currents fed from DERs during a short-circuit (SC) fault. The resulting SC current can be too low to trigger conventional overcurrent relays on distribution feeders, leading to a protection failure (should operate but does not). To address this issue, this paper proposes an intelligent overcurrent protection scheme, which applies a machine learning algorithm innovatively, i.e., the radial basis function neural network (RBFNN), to learn and detect the SC fault currents fed by inverter based DERs (IBDERs) intelligently based on the features of their time series data. This algorithm can be implemented in the microprocessor of a digital relay on a distribution feeder to online detect the SC faults of distribution systems with IBDERs fast and accurately. Numerical simulation has been performed in a distribution system benchmark with IBDER integration to verify the effectiveness of the proposed algorithm.**

Keywords— Inverter based DER, intelligent overcurrent protection, RBFNN, SC fault

I. INTRODUCTION

Worldwide power systems are transitioning to a resource mix that relies less on coal and nuclear while integrating more locally available DERs such as natural gas, wind, and solar photovoltaic (PV) due to vast energy demand and climate impacts [1]. In the last decade, DERs have been greatly promoted due to their various benefits, such as improving the resiliency of power systems, reducing the overall electricity cost, and increasing the efficiency of renewable energy conversion. It is reported that the total capacity of DERs around the world is 158.3 GW in 2019, and will be up to 345 GW by 2028, including 245 GW from solar PV installations [2].

By definition, the DER include both small scale diesel driven synchronous generators and inverter based generation technologies utilizing renewable energy. Despite environmental and economic benefits, the significant penetration of these inverter based DERs (IBDERs) has led to undesired issues to the protection system of distribution systems due to the decline of the SC fault current of distribution feeders [3]. Traditional distribution systems are radial and protected by circuit breakers (CB) on distribution feeders, which are controlled by overcurrent relays. When a SC fault current exceeds the threshold setting of an overcurrent relay, the relay sends a trip signal to the corresponding CB to isolate the fault. The settings of overcurrent relays in distribution systems are determined based on the characteristics of the SC fault current fed from conventional synchronous generators. However, in current distribution systems, the fault current fed from IBDERs has totally different characteristics due to their inverter control. This can cause the malfunction of the conventional overcurrent protection system, leading to significant damage to costly electrical equipment in severe situations.

It is known that the IBDER has a weaker SC fault current feeding capability compared with a conventional synchronous generator [4-5]. In our previous study [6], a quantitative analysis showed that the SC fault current fed from a conventional synchronous generator is about 5 times higher than its current rating. It can be easily recognized and detected by an overcurrent relay. However, the SC fault current fed from an IBDER is much lower and only 1.2 to 1.5 times of its current rating. The main reason is that the SC fault current fed from an IBDER is limited by the current limitation controller of its inverter, which is used to protect power electronic switches of the inverter that are sensitive to a high current. The resulting low SC fault current can be lower than the current setting of an overcurrent relay. As a result, the overcurrent relay fails to activate the corresponding CB to interrupt the SC fault. Even the low SC fault current is slightly beyond a current setting, it still leads to a sluggish operation of the CB tripping due to the inverse time-current characteristics of overcurrent relays [7].

In the existing literature, some researchers have proposed several methods to address the protection issue caused by the penetration of DERs including distributed synchronous generators and IBDERs. A protection scheme is proposed based on predefined protection settings of conventional overcurrent relays for different operation modes, i.e., the grid-connected and island modes of the DERs [8]. However, this method is not efficient for protection systems with high-level penetration of DERs. With the fast development of microprocessors, it is possible to implement computationally intensive algorithms for high speed and accurate detection of fault signals [9]. Reference [10-11] discussed strategies relying on adaptive overcurrent relays to detect faults (normal or high impedance) in distribution systems that cannot be detected due to the integration of DERs into the network. Most of these strategies rely on modifying relay settings according to system operating conditions (i.e., newly connected DERs and actual loading conditions). The methods proposed in [12-13] track and estimate both of the current and voltage, and adaptively choose an optimal current setting for the overcurrent relay in different operation modes of the DERs. However, all the research work mentioned above mainly focused on the protection coordination of the overcurrent relays due to the integration of generally DERs including

978-1-7281-5826-6/20/$31.00 ©2020 IEEE

synchronous generators, and they did not specifically study the impact of the lower fault current fed by the IBDERs.

To the best of the authors' knowledge, the discussed protective issue caused by the integration of IBDERs has not been solved yet. A voltage enhanced current detection method is discussed in [14] to detect the SC fault currents fed from an IBDER. This method added a voltage dip detection function to the overcurrent protective relay to determine a SC fault. However, this protection scheme is not reliable since most of IBDERs in power systems are required to have voltage support capabilities, which can lead to a subtle voltage dip during faults that cannot be detected easily [15].

To address the above issue, this paper proposes an intelligent protection algorithm using the machine learning algorithm innovatively, i.e., RBFNN, to detect the low SC faults fed from IBDERs. By learning the features of time series data of currents during normal and fault conditions in an offline training, the gained model is applied to intelligently detect the SC fault current fed from an IBDER. The proposed algorithm can be implemented in the microprocessor of digital relays to detect faults in real time. In order to generate the training data, a distribution system benchmark with an integrated IBDER is developed to obtain the current data fed from the IBDER under both normal and fault conditions. The RBFNN has been used for the fault diagnosis in many areas due to its excellent performance on the universal optimal approximation and fast learning convergence [16]. However, it is the first time to be applied in power systems for the SC fault current detection.

This paper is organized as follows. Section II discusses the system configuration including a benchmark of a distribution system with an IBDER and the inverter control scheme. Section III discusses the RBFNN and proposes the intelligent overcurrent protection algorithm. Section IV shows a case study to verify the effectiveness of the proposed algorithm. Section V concludes this paper and discusses future work.

II. System Configuration

This paper uses a typical IBDER model, i.e., a grid-connected distributed PV system to generate, to develop a distribution system benchmark.

A. Grid-connected PV system

Fig. 1 shows the sigle-line diagram of a grid conneted distributed PV system in a distribution system. The PV system is mainly composed of a PV array, a large DC-link capacitor and an inverter. The functions of the main components are decribed as follows: (1) the PV array converts solar energy into DC power, which is affected by weather conditions, mainly including temperature and illumination [17]; (2) a large DC-link capacitor between the PV array and the inverter stabilizes the DC link voltage; (3) the inverter can maintain the maximum output power of the PV array and transform the output of DC power into the AC power injected into the grid via its control system; and (4) the LCL filter is used to reduce the total harmonics distortion (THD) of the injected current to the grid.

The inverter is the core component of the PV system, which has a complex control system to achieve its functions. (1) In order to extract the maximum power from the PV array under varying weather conditions, a control strategy maximum power point tracking (MPPT) is applied to control the PV array to work at the maximum power point. (2) The inverter transforms the output of DC power into the AC power and delivered to the grid via its current and voltage control. (3) To ensure the voltage and current phasor are matched with the main grid, a grid synchronization is achieved via a phase-locked loop (PLL) in the inverter controller. The output of the inverter controller is a gate pulse signal generated via a pulse width modulator (PWM).

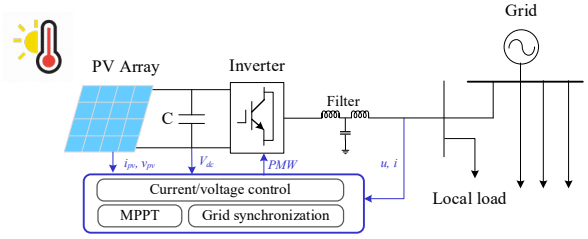

Fig.1: Single-line grid-connected PV system

B. Inverter control strategy

The inverter applies a double-loop control, where the outer loop is to control the DC link voltage to enable the maximum PV output, and the inner loop is a current control loop of the inverter, as shown in Fig.2. The grid synchronization is realized via a PLL control, which generates the grid voltage angle to ensure the output current of the inverter matches with the power grid in phase and frequency.

In order to achieve an easy control of the output power, the three-phase (phase a, b, c) varying voltage and current signals are transformed into constant values including the d-axis components and the q-axis components through Park's transformation [18]. In this way, the actual active power P and reactive power Q could be expressed in (1) and (2).

$$P = V_d I_d + V_q I_q \tag{1}$$

$$Q = V_q I_d - V_d I_q \tag{2}$$

where the symbols $I_d(V_d)$ and $I_q(V_q)$ are the grid currents (voltages) in the d-q coordinate system. In the inner current loop, a decoupling current controller is applied to decouple P and Q, so that they can be controlled separately via the d and q components of the current.

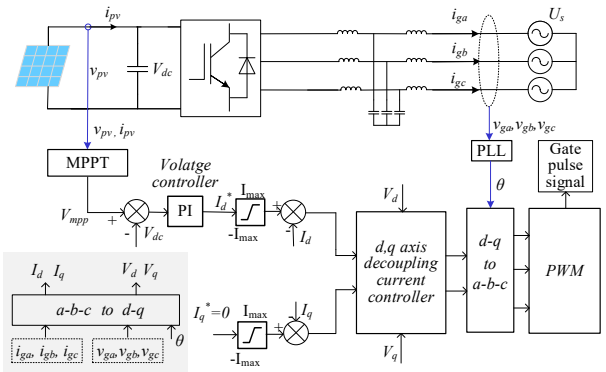

Fig.2 Inverter control strategy

Fig. 2 shows the structure of the inverter control strategy. The symbol V_{mpp} is the output of the MPPT and the symbol V_{dc} is the voltage of the DC-link capacitor. The V_{dc} is subtracted from the reference value V_{mpp} and the result is sent to the PI voltage controller. The output is the reference value $I_d{}^*$ of the d-q axis current. The symbol $I_q{}^*$ is determined by the reactive power delivered to the grid. The value of $I_q{}^*$ is

set to 0 since the grid-connected inverter usually operates in the unit power factor and only provides active power to the main grid.

The current control of the inverter can limit the current fed from an IBDER during a SC fault via a current limiter, which is utilized to avoid the breakdown of the semiconductor devices in the inverter. After passing through the current limiter, the reference current values are subtracted with the actual I_d and I_q, and the result is sent to the d-q axis decoupling controller to generate the signals in the d-q coordinate system. After a reverse Park's transformation to transform the signals in the d-q coordinate system back into the a-b-c coordinate system, the gate pulse control signal is generated via PWM to control the semiconductor switches of the inverter. In order to reduce the impact of grid side voltage disturbances on the current control, the feedforward control of V_q and V_d is added in the inner current loop, which can improve the dynamic response speed of the inverter.

C. Benchmark system

A benchmark of a distribution system with an integrated PV system is developed in this paper for case study, as shown in Fig. 3.

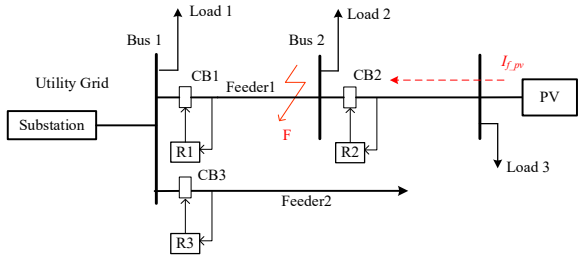

Fig. 3: Benchmark of a distribution system with a PV system

In this system, each feeder segment is protected by a CB controlled by an overcurrent relay. The relays monitor the current flowing through the CBs and activate the CB tripping when the viewed current exceeds its setting [19]. When a fault occurs at point F, both of the fault currents are fed from the main grid and PV system simultaneously. The SC fault current flowing from the main grid is large enough to be detected by Relay R1, which will trip circuit breaker CB1 to isolate the fault from the main grid. However, the SC fault current I_{f_pv} flowing through the circuit breaker CB2 will be limited to a much lower magnitude due to the current limiter of the PV inverter, so that it cannot be detected by Relay R2. As a result, the fault current I_{f_pv} will constantly feed into the fault location. It can result in significant damage of costly electrical equipment such as the inverter and the transformer in the PV system. Most of IBDERs have a current limiter in the current control loop of inverters. It can limit the fault current fed from IBDERs and make this fault current difficult to be detected by overcurrent relays. Therefore, it is necessary to develop an intelligent protection algorithm to detect the low SC fault current from the IBDER fast and effectively.

III. Proposed Protection Scheme

To detect low SC current fed from an IBDER, an intelligent overcurrent protection algorithm applying the RBFNN is proposed in this section.

A. Radial Basis Function Neural Network (RBFNN)

RBFNN is a three-layer neural network (including the input layer, the hidden layer and the output layer), which uses the linear combination of radial basis functions [20]. Due to its simple structure, fast convergence rate and universal optimal approximation ability, RBFNN is widely applied in the pattern classification, function approximation, data mining, etc.

A radial basis function refers to any real-valued function, whose value only depends on the Euclidean distance between the input and some fixed point, i.e., centers. The generally used radial basis function is the Gaussian function represented in (3).

$$\phi(\|x - x_i\|) = \exp\left(\frac{\|x-x_i\|^2}{2\sigma^2}\right) \tag{3}$$

where the symbol x is the input, the symbol x_i is the center and the symbol σ represents the standard deviation, which is also defined as the RBF width parameter.

The function approximation is usually achieved by the radial basis functions in the form of the RBFNN as (4),

$$y(x) = \sum_{i=1}^{N} W_i \ \phi(\|x - x_i\|) \tag{4}$$

where the approximating function $y(x)$ is the output of the RBFNN, represented as a sum of N radial basis function unit, and each unit is associated with a different center x_i and weighted by an appropriate coefficient ω_i. The weights ω_i can be estimated using the matrix method of linear least mean squares (LMS), since the approximating function is linear in the weights ω_i.

The function approximation process is interpreted as a RBFNN, whose structure is shown in Fig.4. The hidden layer applies nonlinear radial basis function units as neurons, which can directly map the input vector without weights for connection. The mapping from the hidden layer to the output layer is linear. That is, the output of the network is the linear weighted sum of the outputs of hidden units, where the weights are adjustable parameters of the network. Therefore, the mapping from the input to the output of the network is nonlinear, while the output of the network is linear. As a result, the weights of the network can be solved directly by the linear equations, which can greatly speed up the learning rate and avoid the local optimal solution problems.

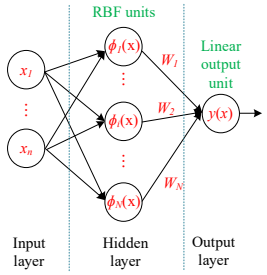

Fig.4 RBFNN structure

The RBFNN training is to generate the optimal two sets of parameters including: (1) the parameters of hidden layers including the center of each RBF units, the RBF width, and the number of hidden layer neurons; and (2) the weights between the hidden layer and the output layer. Generally, the centers can be generated by an unsupervised training, such as k-means clustering. With the determined centers, the RBF width can be determined via (5)

$$\sigma_i = \frac{C_{max}}{\sqrt{2h}} \quad i = 1, \dots, h \tag{5}$$

Where the symbol C_{max} is the maximum distance between the selected centers and h is the number of hidden layer units.

The connection weights of neurons between the hidden layer and the output layer are determined by a supervised method, i.e., gradient descent, which can be directly calculated by the least mean square LMS through (6)

$$\boldsymbol{W} = (\boldsymbol{\Phi}^T\boldsymbol{\Phi})^{-1}\boldsymbol{\Phi}^T\boldsymbol{d} \quad (6)$$

where the symbols $\boldsymbol{W}$ and $\boldsymbol{\Phi}$ are the wight and RBF unit matrix respectively, and the symbol $\boldsymbol{d}$ is the expected output vector in the training data.

B. Intelligent overcurrent protection algorithm

Fig. 5 shows the proposed intelligent overcurrent protection algorithm based on the RBFNN. Through an offline training, the trained RBFNN can be implemented in the microprocessor of a relay on the connecting feeder of the PV system to intelligently detect the SC fault current fed from a PV system in real-time.

During system operation, the time series current signals are sent to relays continuously from the current transformer (CT). In order to generate a training dataset for the offline training of the RBFNN, both of the healthy current sample data during normal operation and SC fault current sample data in a time interval of one cycle (16ms) are collected from the recorded current data. This training dataset consists of five statistical features, which are explained as follows [21].

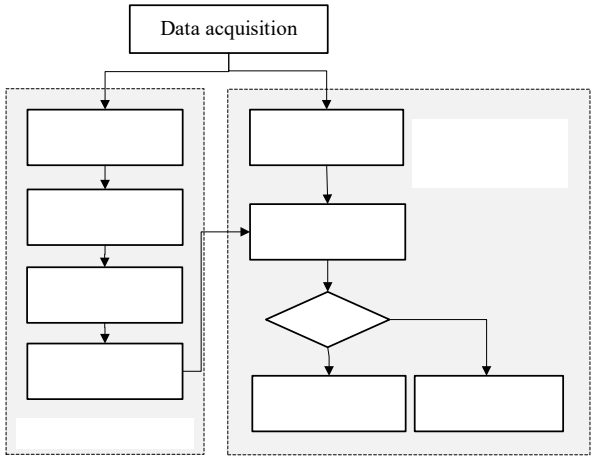

Fig. 5 Intelligent overcurrent protection relay algorithm using RBFNN

(1) ***Range*****:** Range refers to the difference between the maximum and minimum value of a sample data.

(2) ***Mean value*****:** The average value of a sample data is termed as the mean value.

(3) ***Standard deviation*****:** Standard deviation is a measure of the degree of dispersion of the current sample data, as expressed in (7).

$$standard\ deviation = \sqrt{\frac{n\sum x^2-(\sum x)^2}{n(n-1)}} \quad (7)$$

where the symbol x is the sample data set and the symbol n is the sample number.

(4) ***Skewness*****:** Skewness is a measure of symmetry, or more precisely, the lack of symmetry of a time series signal, which is calculated in (8).

$$skewness = \frac{n}{(n-1)(n-2)}\sum(\frac{x_i-\bar{x}}{s})^4 \quad (8)$$

where the symbol $\bar{x}$ is the data mean and the symbol s is the sample standard deviation.

(5) ***Kurtosis*****:** Kurtosis is a measure of the shape of the data to determine whether the data is peaked or flat with respect to a normal distribution, as presented in (9).

$$kurtosis = \frac{n(n+1)}{(n-1)(n-2)(n-3)}\sum(\frac{x_i-\bar{x}}{s})^4 - 3\frac{(n-1)^2}{(n-2)(n-3)} \quad (9)$$

The output values of the RBFNN in the training dataset are defined as the healthy sample data labeled as (1, 0) and the SC fault current sample data labeled as (0, 1). The obtained trained RBFNN model is used to process the test current dataset. When this algorithm outputs "1" in the first value of the label, a fault is detected. Then the relay will send a tripping signal to activate the CB tripping for isolating the fault. Otherwise, the first value of the label stays with "0" that does not trigger any operation.

IV. CASE STUDY

In order to verify the effectiveness of the proposed intelligent overcurrent protection algorithm, a case study is conducted in the developed distribution system benchmark in section II. A fault scenario with the proposed algorithm is reported in this section. Their simulation results are compared with that of the same scenario with the traditional overcurrent relay.

A. Fault detection with traditional overcurrent relay

The fault detection with traditional overcurrent relays is carried out in the developed distribution system benchmark in Fig.3, where the voltage of the feeder 1 is 10.48kV, the load on feeder 1 is 90kW and the output power of the PV system is 46kW. The minimum current setting of a traditional overcurrent relay is normally 1.5 to 2 times of the current rating [7]. When a fault occurs at 0.5s at point F, the SC fault current viewed by Relay R2 is shown in Fig. 6.

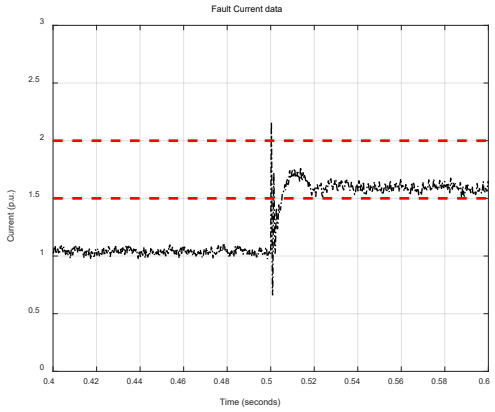

Fig. 6 SC fault current fed from the PV system

It shows that during the fault, this SC fault current fed from the PV system fluctuates and decreases to 1.6 per unit (p.u.) due to the current limitation. It cannot be detected by the relay with a setting higher than 1.6 p.u.. Even the relay setting is lower than 1.6 p.u. and the fault is detected, the operation of the time inverse overcurrent relay will be sluggish with a large time delay due to the narrow margin

between the SC fault current and the current setting. This long-lasting SC fault can result in severe device damage.

B. Fault detection with proposed protection algorithm

Based on the proposed protection algorithm, the training dataset needs to be generated for the offline training of the RBFNN. The SC fault current data flowing through CB2 in one cycle time window is collected and recorded by Relay R2 in real-time. Four fault scenarios are developed in this paper to generate four datasets of the SC fault current with the Fault F on Feeder 1 located at 5 km, 10 km, 15 km and 20 km away from Bus 2 in Fig. 3 (the line impedance is given as 0.35 Ω/ km). Fig. 7 shows the current dataset with the fault location at 5 km from Bus 2 as an example.

As shown in Fig.7, two data samples are selected from each current dataset to generate the offline training datasets, including a healthy current data sample that is randomly selected in a one-cycle interval, say from 0.42s to 0.436s, and a SC fault current data sample that is selected in a one-cycle interval from 0.5 s to 0.516 s. Accounting four fault scenarios, eight data samples in total are included in the training datasets, which have the extracted features, including the range, mean value, standard derivation, skewness and kurtosis. These features and labels listed in TABLE I are the inputs and outputs of the RBFNN, respectively. Using the training datasets, the RBFNN model is trained to approximate the feature mappings of the current data in both normal and fault situations.

To test the overcurrent algorithm with the trained RBFNN, we developed four more fault scenarios with the Fault F on Feeder 1 located at 4 km, 8 km, 12 km and 16 km away from Bus 2. Similar to the process of generating the training datasets, eight test data samples including four healthy current samples and four fault current samples are

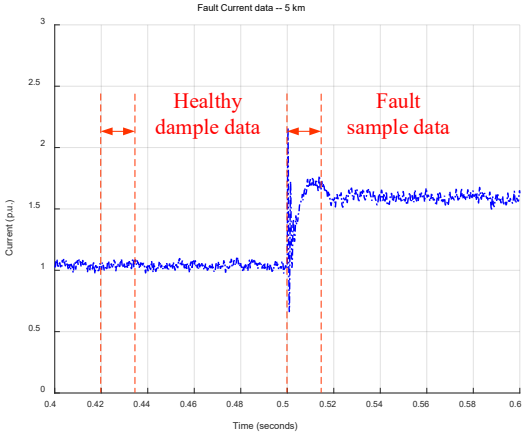

Fig. 7 Current sample data

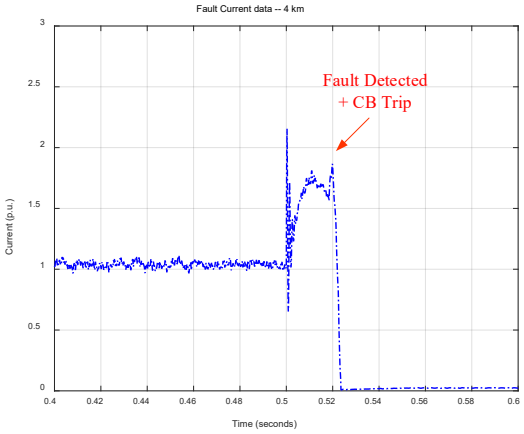

Fig. 8 Test of trained RBFNN

TABLE I. TRAINING DATASET

Features	***Training data***							
	SC fault current data				***Healthy current data***			
Range (p.u.)	1.589	1.590	1.586	1.588	1.039	1.038	1.039	1.038
Mean value (p.u.)	1.502	1.500	1.500	1.518	0.125	1.500	1.518	0.125
Standard deviation (p.u.)	0.133	0.131	0.131	0.133	0.024	0.022	0.025	0.025
Skewness	-2.916	-3.130	-3.039	-3.105	-0.058	0.036	-0.082	-0.163
Kurtosis	18.926	20.006	19.602	20.136	2.613	2.634	2.796	2.700
Label	**(1, 0)**	**(1, 0)**	**(1, 0)**	**(1, 0)**	**(0, 1)**	**(0, 1)**	**(0, 1)**	**(0, 1)**

TABLE II. TEST RESULTS

Features	***Test current data***							
	SC fault current data				***Healthy current data***			
Range (p.u.)	1.591	1.587	1.589	1.586	1.038	1.037	1.039	1.038
Mean value (p.u.)	1.503	1.531	1.503	1.531	0.139	0.131	0.133	0.143
Standard deviation (p.u.)	0.135	0.135	0.129	0.133	0.025	0.023	0.0230	0.025
Skewness	-2.861	-2.988	-3.195	-2.863	0.043	0.089	0.062	0.036
Kurtosis	18.256	19.050	21.245	18.767	2.804	2.757	2.967	2.849
Output	**(1, 0)**	**(1, 0)**	**(1, 0)**	**(1, 0)**	**(0, 1)**	**(0, 1)**	**(0, 1)**	**(0, 1)**
Signal for tripping	**1**	**1**	**1**	**1**	**0**	**0**	**0**	**0**

selected from the currents of these four fault scenarios. The features of these current samples are abstracted and then function as inputs of the RBFNN. Using the trained RBFNN, the label outputs indicating whether the selected test data samples are in healthy or fault conditions are determined. The corresponding tripping signals sent by Relay R2 during these fault scenarios are also recorded. All the features, the label outputs of these test data samples, and the tripping signals are reported in TABLE II. The detection results show that all the four SC fault current data samples are detected accurately with the outputs (1,0), and these faults are successfully isolated by sending the trip signal "1" to CB2. The healthy current data samples are also detected with the label output of (0,1) and the tripping signal of 0, which leads to no operation of CB2. One of fault test scenarios are reported in Fig. 8 as an example, i.e., the fault current flowing through CB2 with the proposed algorithm applied in Relay R2 and Fault F located at 4 km away from Bus 2. It is seen that the fault current became 0 at 0.52 s that is about one cycle after the fault occurrence at 0.5 s with together the calculating time delay. It is indicated that this SC fault is successfully detected and isolated.

The offline training time for the RBFNN is 0.414 seconds and the detection time of the proposed algorithm using the trained RBFNN is 0.0136 seconds (less than one cycle) on a lab platform including an intel core i7 2.6GHz CPU, an NVIDIA GTX 950M GPU, and 8GB RAM. This algorithm can be easily implemented in the microprocessor relays. The simulation results demonstrate that the proposed intelligent overcurrent protection algorithm can detect the SC faults in distribution system with IBDERs fast and accurately.

V. CONCLUSIONS

This paper proposes an intelligent overcurrent protection algorithm applying the RBFNN to learn and detect the SC fault current fed from IBDERs. This fault current is limited by the inverter control and therefore difficult to be detected by a conventional overcurrent relay. A case study shows that the proposed algorithm can detect the low fault current fed by an IBDER in a distribution system fast and accurately. The proposed algorithm can be easily implemented in a digital relay for online detection of the low fault current. In the future, we will develop an advanced intelligent protection scheme for distribution systems with IBDER integration. A deep learning method will be applied to improve the robustness and universality of the protection algorithm. The effectiveness of this algorithm will be verified in the real-time simulator OPAL-RT.

REFERENCES

[1] "EU Energy Policy to 2050: Achieving 80-95% emissions reductions," European Wind Energy Association, pp. 68, Mar. 2011.

[2] "Global DER Overview: Market Drivers and Barriers, Technology Trends, Competitive Landscape, and Global Market Forecasts", Navigant Research, Chicago, IL, U.S.. June 2019.

[3] J. Driesen and F. Katiraei, "Design for distributed energy resources," *IEEE Power Energy Mag.*, vol. 6, no. 3, pp. 30-40, June 2008.

[4] J. Keller and B. Kroposki, "Understanding Fault Characteristics of Inverter-Based Distributed Energy Resources," National Renewable Energy Laboratory (NREL), Golden, CO, U.S.. Rep. TP-550-46698, January 2010.

[5] A. Hooshyar and R. Iravani, "Microgrid Protection," *Proceedings of the IEEE*, vol. 105, no. 7, pp. 1332-1353, July 2017.

[6] S. Rong and L. He, "Impact of Integration of Photovoltaic Generation on Protection of Distribution Systems", in *Proc. MIT A+B Applied Energy Symposium*, 2020. Accepted.

[7] J. L. Blackburn and T.J. Domin. *Protective relaying: principles and applications.*3rd ed. CRC press, Boca Raton, FL, U.S., 2006.

[8] P. Mahat, C. Zhe, B. Bak-Jensen, and C. L. Bak, "A simple adaptive overcurrent protection of distribution systems with distributed generation," *IEEE Trans. Smart Grid*, vol. 2, no. 3, pp. 428–437, Sep. 2011.

[9] M. S. Sanchdev and R. Das. "Understanding microprocessor based technology applied to relays", IEEE power system relaying committee, Rep. WG I01, Jan. 2009.

[10] A. Conde and E. Vazquez, "Operation logic proposed for time overcurrent relays," *IEEE Trans. Power Del.*, vol. 22, no. 4, pp. 2034–2039,Oct. 2007.

[11] D. S. Kumar, D. Srinivasan and T. Reindl, "A Fast and Scalable Protection Scheme for Distribution Networks With Distributed Generation," *IEEE Trans. Power Del.*, vol. 31, no. 1, pp. 67-75, Feb. 2016.

[12] A. D. Oliveira, L. R. M. Silva, C. H. Martins, etc., "An improved DFT based method for phasor estimation in fault scenarios," i*n Proc. IEEE Pow. Eng. Soc. Gen. Meet.,* San Diego, CA, USA, Jul. 2012, pp. 1–5.

[13] H. Wen, S. Guo, Z. Teng, and F. Li, "Frequency estimation of distorted and noisy signals in power systems by FFT-based approach," *IEEE Trans. Power Syst.*, vol. 29, no. 2, pp. 765–774, Mar. 2014.

[14] A. Agrawal, M. Singh and M. V. Tejeswini, "Voltage current based time inverse relay coordination for PV feed distribution systems," *NPSC*, Bhubaneswar, 2016, pp. 1-6.

[15] N. Mahmud and A. Zahedi. "Review of control strategies for voltage regulation of the smart distribution network with high penetration of renewable distributed generation", *Renew. Sust. Energy Rev.*, vol. 64, pp. 582-595, Oct. 2016.

[16] C. M. Bishop, *Pattern Recognition and Machine Learning*, Springer Science Business Media, New York, NY, USA, 2006.

[17] X. H. Nguyen and M .P. Nguyen, "Mathematical modeling of photovoltaic cell/module/arrays with tags in Matlab/Simulink", *Environmental Systems Research.*, pp. 1-13, 2015.

[18] A. V. Sant, V. Khadkikar, W. Xiao, H. Zeineldin and A. Al-Hinai, "Adaptive control of grid connected photovoltaic inverter for maximum VA utilization," in *Proc. Annu. Conf. IEEE Industrial Electron. Soc.*, Vienna, 2013, pp. 388-393.

[19] M. Kezunovic, J. Ren and S. Lotfifard, Design, *Modeling and Evaluation of Protective Relays for Power Systems*, Springer International Publishing, Switzerland, 2016.

[20] J. Park and I. W. Sandberg, "Universal Approximation Using Radial-Basis-Function Networks", *Neural Compu.*, vol. 3 no. 2, pp. 246-257, 1991.

[21] P. K. Kankar, S. C. Sharma and S. P. Harsha, "Fault diagnosis of ball bearings using machine learning methods", *Expert Syst. Appl.*, vol. 38, no. 3, pp. 1876-1886, Mar. 2011.

Lina He received the Ph.D. degree in electrical engineering at University College Dublin, Ireland in 2014, and the B.S. and M.S. degrees from Huazhong University of Science and Technology, China, in 2007 and 2009, respectively. She is currently an Assistant Professor in department of electrical and computer engineering, University of Illinois at Chicago, Chicago, USA. She was a Project Manager and Senior Consultant at Siemens headquarter in Germany and Siemens US from 2014 to 2017. She was also an Electrical Engineer at State Grid Corporation of China from 2009 to 2010. Her research interests include modeling, control and protection of power electronics based power systems, HVDC control and operation, renewable energy integration, and wide-area protection and cybersecurity.

Shuaiang Rong received the B.S degree in Automation in 2015 and M.S. degree of electric engineering in 2018 both from Shanghai University of Electric Power. She is currently pursuing Ph.D. degree in electrical engineering at the University of Illinois at Chicago, Chicago, USA. Her research interest includes machine learning, renewable energy integration and power system protection.